ACS OMEGA

http://pubs.acs.org/journal/acsodf

Article

Comparison of cRGDfK Peptide Probes with Appended Shielded Heptamethine Cyanine Dye (s775z) for Near Infrared Fluorescence Imaging of Cancer

Rananjaya S. Gamage, Dong-Hao Li, Cynthia L. Schreiber, and Bradley D. Smith*

Cite This: *ACS Omega* 2021, 6, 30130−30139

Read Online

ACCESS | Metrics & More | Article Recommendations | Supporting Information

ABSTRACT: Previous work has shown that the sterically shielded near-infrared (NIR) fluorescent heptamethine cyanine dye, **s775z**, with a reactive carboxyl group produces fluorescent bioconjugates with an unsurpassed combination of high photostability and fluorescence brightness. This present contribution reports two new reactive homologues of **s775z** with either a maleimide group for reaction with a thiol or a strained alkyne group for reaction with an azide. Three cancer-targeting NIR fluorescent probes were synthesized, each with an appended cRGDfK peptide to provide selective affinity for integrin receptors that are overexpressed on the surface of many cancer cells including the A549 lung adenocarcinoma cells used in this study. A set of cancer cell microscopy and mouse tumor imaging experiments showed that all three probes were very effective at targeting cancer cells and tumors; however, the change in the linker structure produced a statistically significant difference in some aspects of the mouse biodistribution. The mouse studies included a mock surgical procedure that excised the subcutaneous tumors. A paired-agent fluorescence imaging experiment co-injected a binary mixture of targeted probe with 850 nm emission, an untargeted probe with 710 nm emission and determined the targeted probe's binding potential in the tumor tissue. A comparison of pixelated maps of binding potential for each excised tumor indicated a tumor-to-tumor variation of integrin expression levels, and a heterogeneous spatial distribution of integrin receptors within each tumor.

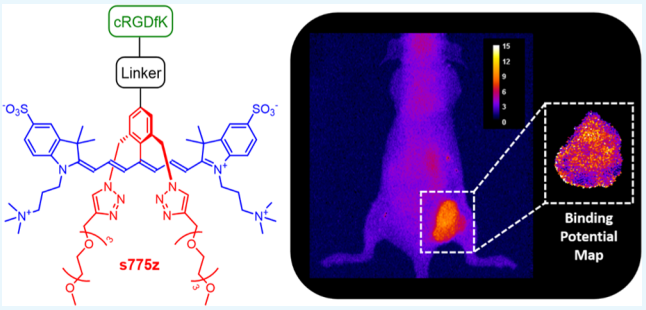

INTRODUCTION

A common synthetic chemistry method to produce a fluorescent molecular probe is to covalently attach a fluorescent dye to a peptide-based targeting unit that has strong and selective affinity for a biomarker.[1−3] Molecular probes containing near-infrared (NIR) fluorescent dyes are especially valuable for *in vivo* fluorescence imaging because there is deep penetration of NIR light through skin and tissues, lower scattering of NIR light, and minimal background autofluorescence.[4−6] However, the relatively large size and polyanionic charge of most fluorescent NIR dyes can compromise the probe's tumor-targeting efficiency and probe pharmacokinetics.[7−11] This is a common problem with heptamethine cyanine dyes (often referred to as Cy7 dyes) because they have large amounts of hydrophobic surface area which promotes self-aggregation and non-selective affinity with off-target biological surfaces. Compounding this performance drawback is the inherent chemical reactivity of Cy7 dyes, along with sensitivity to photobleaching under photon-intense imaging conditions. Efforts to obviate each of these chemical and photophysical limitations has led to modified Cy7 dyes with rigidified polyene chains,[12−15] linkers with increased chemical stability,[16] and a geometric distribution of opposing charges (zwitterionic Cy7 dyes).[17−20]

We have contributed to this Cy7 probe optimization effort by designing a new class of heptamethine cyanine dyes that we call shielded Cy 7 dyes.[21,22] The prototype example is **s775z** (Scheme 1), which has two short triethylene glycol arms (colored red) that shield each face of the heptamethine fluorochrome (colored blue). The shielding arms prevent dye self-aggregation, but they do not weaken association of bioconjugates with their targets. For example, the fluorescent molecular probe **s775z-aRGD** is a conjugate with an appended cyclic peptide (cRGDfK) that contains a rigidified Arg-Gly-Asp recognition motif for integrin receptors that are over expressed on the surface of many cancer cells,[23] and we have previously shown that **s775z-aRGD** enables NIR fluorescence imaging of tumors in a subcutaneous mouse model of cancer.[21]

Received: September 9, 2021
Accepted: October 21, 2021
Published: October 30, 2021

Scheme 1. Chemical Structures of the Dyes and Fluorescent Molecular Probes Used in this Study[a]

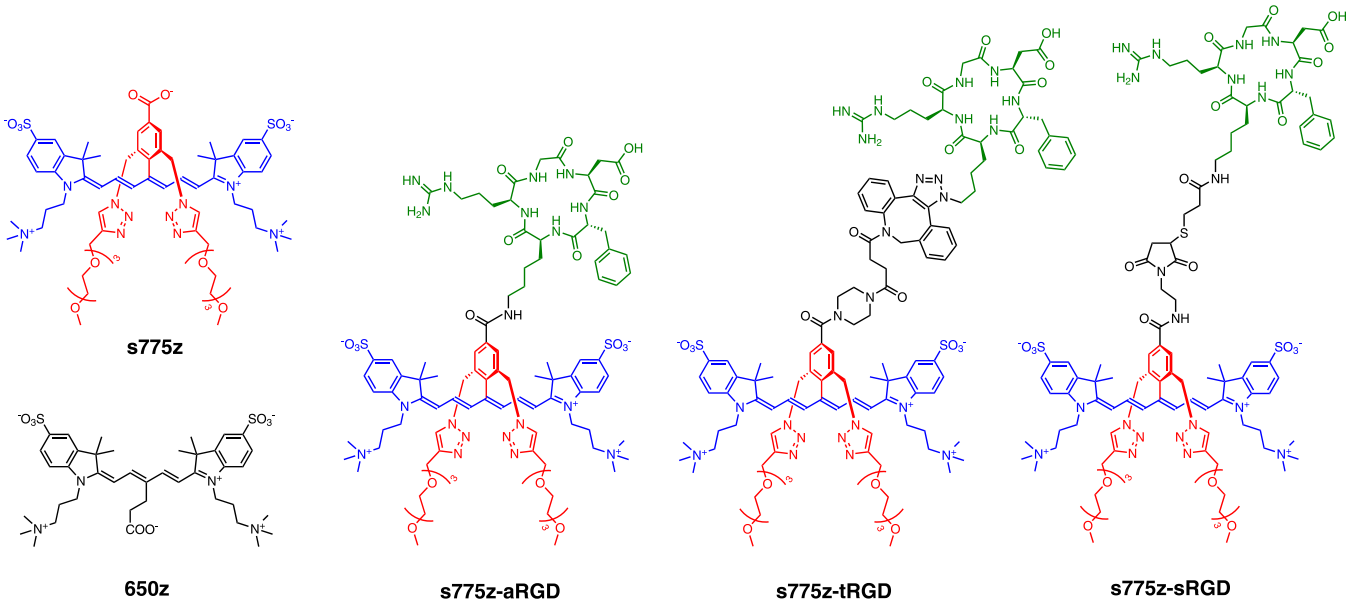

[a]The structures of three fluorescent molecular probes, **s775z-aRGD**, **s775z-tRGD**, and **s775z-sRGD**, are comprised of three colored-coded components; the targeting cRGDfK peptide (green) is connected to the **s775z** dye (red and blue) by a linker (black). The abbreviations for the three linkers in the probe descriptor names are amide (a) triazole (t), and thiol (s).

Scheme 2. Synthesis of Fluorescent Molecular Probes s775z-aRGD, s775z-tRGD, and s775z-sRGD, which Differ by the Linker (Black) Connecting the s775z Dye (Red and Blue) to the Targeting cRGDfK Peptide (Green), as Illustrated by the Chemical Structures in the Boxes on the Right

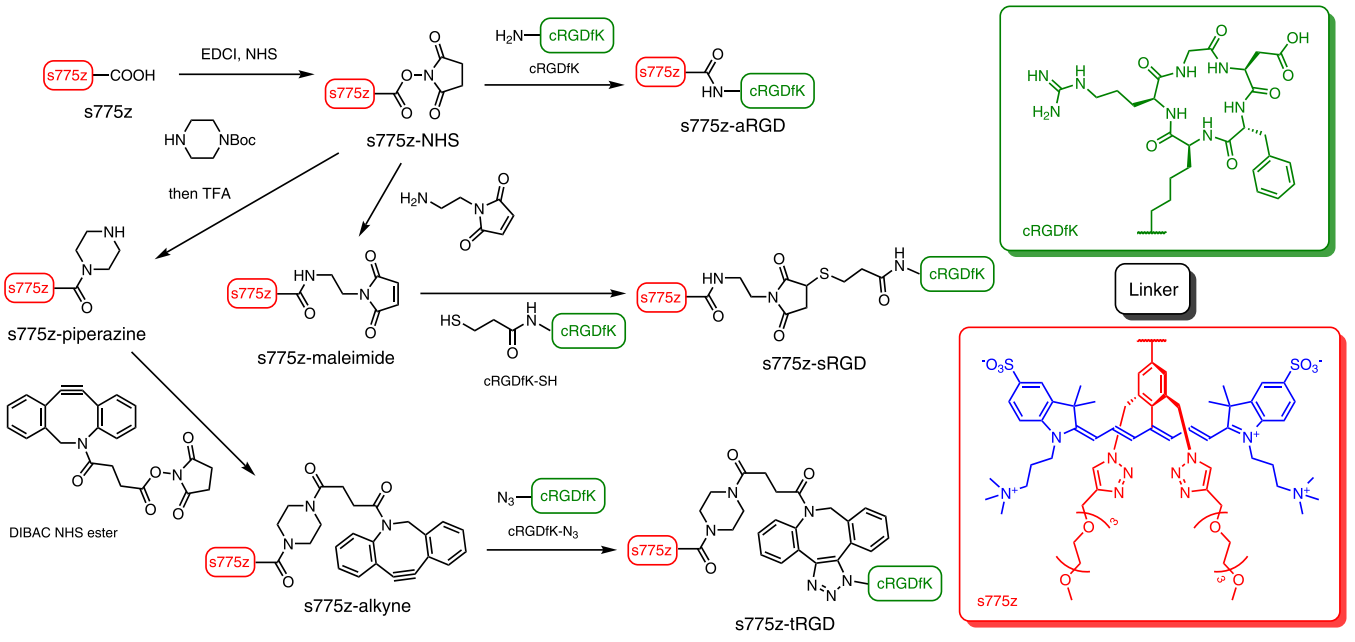

The structure of **s775z** has a reactive carboxylic acid and the bioconjugation process to make **s775z-aRGD** was mediated by a coupling reaction with an amine residue on the targeting cRGDfK peptide. We wanted to extend the scope of bioconjugation reactions that can be conducted using **s775z**; and herein, we report two new reactive homologues, namely, **s775z-maleimide** which reacts spontaneously with a thiol group, and **s775z-alkyne** which reacts spontaneously with an azide group.[24] In addition to demonstrating the high synthetic efficiency of the new bioconjugation reactions, we have evaluated the effect of the different bioconjugation linkers on targeted imaging performance. To ensure a direct and unambiguous comparison, we maintained the same cRGDfK targeting unit and quantified the imaging performance of the three molecular probes shown in Scheme 1. The imaging studies included cell microscopy and mouse tumor imaging experiments. Moreover, the *in vivo* imaging studies utilized a paired-agent imaging (PAI) as an efficient and informative method to quantify the extent and heterogeneity of integrin targeting within the tumor tissue.[25] The results indicate that all

https://doi.org/10.1021/acsomega.1c04991
ACS Omega 2021, 6, 30130−30139

Table 1. Spectral Properties of Fluorescent Probes in pH 7.4 PBS Buffer at Room Temperature[a]

Dye	λ_{max}^{abs} (nm)	λ_{max}^{em} (nm)	SS (nm)	ε (M^{-1} cm^{-1})	R^2	Φ_F (%)[b]	brightness[b]
s775z	775	794	19	201,000	0.999	9.0	18,000
s775z-aRGD	776	796	20	190,000	0.999	8.1	15,000
s775z-sRGD	776	796	20	200,000	0.996	8.2	16,000
s775z-tRGD	776	797	21	170,000	0.995	8.1	14,000
650z	640	659	19	270,500		22.5	61,000

[a]SS is the Stokes shift, ε is molar absorptivity, Φ_F is fluorescence quantum yield, brightness = $\varepsilon \times \Phi_F$. [b]Estimated error is ±10%.

three fluorescent probes are highly effective at cancer targeting although there is a statistically significant difference in some aspects of the mouse biodistribution.

RESULTS AND DISCUSSION

Synthesis and Spectral Properties. Scheme 2 summarizes the synthetic pathways that convert **s775z** into the different targeted fluorescent probes. We had previously used **s775z-NHS** for amide-based conjugation and while the chemistry with this reactive dye is straightforward, the slow water reactivity of the NHS ester group must be kept in mind during reaction planning.[21] With regard to the new conjugation chemistry in this present study, **s775z-maleimide** was reacted with cRGDfK-SH[26] to make **s775z-sRGD** in 64% yield, and **s775z-alkyne,** and it was reacted with cRGDfK-N_3[27] to make **s775z-tRGD** in 90% yield. It is important to emphasize that **s775z-maleimide** and **s775z-alkyne** are stable over long-term storage, and their specific bioconjugation reactions occur spontaneously in good to high yield at room temperature in water. Moreover, the conjugation reactions are biorthogonal; that is, they proceed selectively in the presence of a large excess of competing biological nucleophiles. Thus, **s775z-maleimide** and **s775z-alkyne** will be broadly useful as NIR dye-labeling reagents for a range of fluorescence imaging and diagnostics technologies.[1,24,28] The other fluorophore system in Scheme 1 is the zwitterionic pentamethine cyanine probe **650z** which was synthesized according to a literature procedure[29] and used in this project as an untargeted fluorescent probe for the PAI experiments. The absorption and fluorescence emission spectra of all the probes are provided in Figure S16 and the spectral properties are listed in Table 1. Most importantly, the absorption spectra show no evidence for band broadening due to probe self-aggregation, and the three homologous s775z probes (**s775z-aRGD**, **s775z-tRGD**, and **s775z-sRGD**) have very similar fluorescence brightness. Additional physiochemical properties of the probes are provided in Table S1.

Albumin Binding and Cell Studies. The shielding arms (colored red) within the NIR fluorescent s775z probes have two main purposes. One is to prevent probe self-aggregation and the other is to decrease undesired probe association with off-target biological surfaces such as the abundant blood serum proteins. This latter property was measured by conducting a series of separate fluorescence titration experiments that added aliquots of one of the s775z probes to a solution of bovine serum albumin (BSA) and monitored the quenching of the sole BSA tryptophan residue.[30] Titration isotherms along with the curve fitting details are shown in Figure S17. In short, the BSA association constant for the unconjugated dye **s775z** was determined to be $K_a = 2.7 \times 10^4$ M^{-1} at 37 °C, and for the three targeted **s775z** conjugates, K_a was in the range of 4.0−7.0 $\times 10^4$ M^{-1}. These values are all quite similar and more than ten times lower than the BSA association constant for the benchmark cyanine dye, indocyanine green (ICG).[30] Moreover, the BSA affinity of the three cRGDfK conjugates is much weaker than the affinity of the cRGDfK targeting unit for cell surface integrin receptors.[31] Thus, BSA association was not expected to attenuate the cancer cell targeting properties of the three homologous cRGDfK probes.

A series of cytotoxicity and cell microscopy experiments were conducted using A549 lung adenocarcinoma cells that we have previously verified by immunofluorescence methods to overexpress $\alpha_v\beta_5$ integrin receptors with high affinity for the cRGDfK targeting unit.[21,25,31] Cell viability experiments employed a standard MTT assay that incubated a population of cells with increasing amounts of the probes for 24 h. As shown in Figure S18, probe concentrations up to 30 μM (highest concentration tested) induced no changes in cell viability over 24 h and previous studies have shown that the unconjugated dye **s775z** has no affinity for the cells and induces no cell toxicity.[21] Representative fluorescence micrographs of A549 cells that were treated with the three targeted s775z probes are shown in Figure 1a. The micrographs and associated quantification data in Figure 1b show that all three targeted s775z probes were taken up by the cells and that probe uptake was blocked by the presence of free cyclic peptide cRGDfK which competed for the integrin receptor binding pocket.

Mouse Cancer Imaging. The high levels of the targeted NIR fluorescent probe uptake by the cultured A549 cells prompted us to evaluate fluorescence imaging performance in a mouse subcutaneous tumor model. Typically, this type of mouse imaging study examines two separate cohorts of mice that have been dosed with either an untargeted or a targeted fluorescent probe and assesses if there is a difference in the mouse biodistribution.[25] A drawback with this conventional single agent imaging experiment is the inherent variability in imaging signals due to the individual changes in tumor size and depth, along with differences in the extent and integrity of the tumor vascularization. This often means that large cohort numbers must be evaluated to ensure a statistically relevant difference.[5,32,33] To mitigate the mouse-to-mouse tumor variation, we evaluated the tumor targeting properties of the three s775z probes by conducting a set of mouse PAI experiments.[25,34−36] The PAI approach injects a dose that is a binary mixture of spectrally distinct, untargeted, and targeted fluorescent probes. Simultaneous imaging at the two distinct wavelengths enables the initial image of the targeted fluorescent probe to be corrected by subtracting the image signal caused by untargeted probe accumulation.[25,34−36] The PAI correction eliminates imaging artifacts due to dynamic tissue retention effects and it is an efficient way to quantify *in vivo* tumor targeting performance using relatively small cohort numbers.[35,37]

A set of PAI experiment intravenously injected separate cohorts of nude mice, each bearing a subcutaneous A549

https://doi.org/10.1021/acsomega.1c04991
ACS Omega 2021, 6, 30130−30139

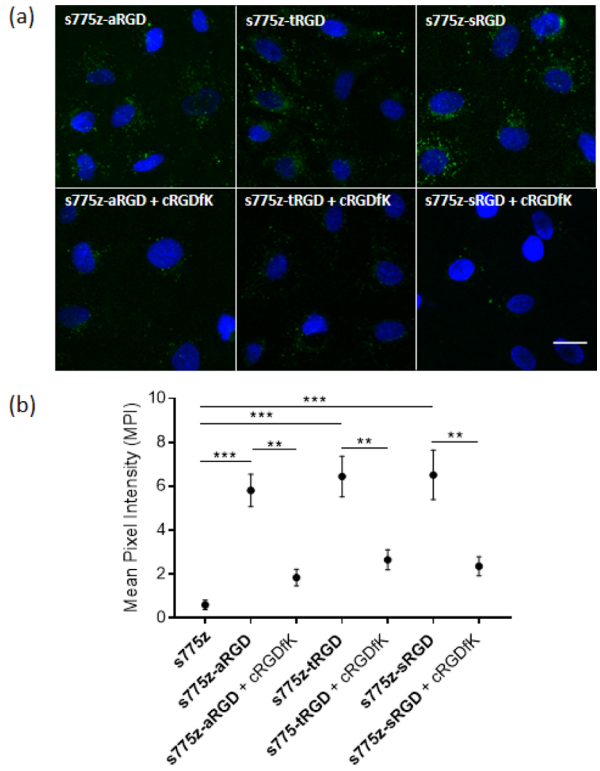

Figure 1. (a) Representative fluorescence micrographs of human A549 lung adenocarcinoma cells treated with 10 μM of one of the targeted probes; **s775z-aRGD**, **s775z-tRGD,** or **s775z-sRGD**. Probe uptake by the cells was blocked by incubating the cells with 200 μM of free cRGDfK for 20 min prior to the addition of the fluorescent probe. In each experiment, probe addition to the cells was followed by cell fixation with paraformaldehyde and treatment with the Hoechst nucleus stain. The probe NIR fluorescence (ex: 769/41 nm, em: 832/37 nm) is pseudo-colored in green for enhanced image contrast and the Hoechst fluorescence (ex: 387/11 nm, em: 447/60 nm) in blue. Length scale = 30 μm. (b) Quantification of cell micrograph fluorescence intensity. ** indicates $p < 0.01$ and *** indicates $p < 0.001$.

tumor in the right rear flank, with a binary mixture comprised of the untargeted probe **650z** that emits fluorescence at 710 nm, and one of the three targeted fluorescent s775z probes with 850 nm emission. Fluorescence images of syringes containing diluted solutions of each probe alone or 1:1 binary mixture showed that the 710 and 850 nm emission wavelengths could be distinguished using the appropriate filter sets on a standard *in vivo* imaging station (Figure S19). It is worth emphasizing that the untargeted probe **650z** is a low molecular weight pentamethine cyanine dye with very high fluorescent brightness (Table 1) and its chemical structure possesses an equal number of anionic and cationic residues—structural features that ensure **650z** has a very low nonspecific affinity for biological surfaces and that it is rapidly excreted through the kidney.Representative fluorescence images of three tumor-bearing mice dosed with a binary mixture of targeted and untargeted probes are shown in Figure 2, and imaged periodically over 3 h. As expected, the images show early accumulation of the untargeted **650z** in the tumor followed by washout, such that there is little **650z** remaining in the tumor at 3 h. In contrast, significant amounts of all three targeted NIR fluorescent s775z probes are retained in the tumor at the 3 h time point, with an extensive probe clearance from the bloodstream combining to produce a high tumor-to-background ratio. Plots of the change in tumor fluorescence mean pixel intensity (MPI) and the tumor-to-background ratios for the live mouse images (Figure S20) show that there was slightly more **s775z-tRGD** in the tumor than the other two probes, but the background signal was also higher; thus, the tumor-to-background ratios for all three probes in the living mice were about the same. At the 3 h time point, the mice were sacrificed and a mock surgery was performed to demonstrate the potential of these targeted probes to facilitate a fluorescence-guided surgery (Figure S21).

Probe biodistribution in the euthanized mice was determined by drawing blood from the heart and systematically harvesting the tumors and major organs. Fluorescence imaging of each excised tissue at the 710 and 850 nm emission wavelengths enabled determination of the MPI which was assumed to correlate with the tissue concentration of untargeted or targeted probe, respectively.[38] All the major organs showed very low tissue retention of the untargeted **650z** probe. The low skin accumulation of zwitterionic **650z** is a very useful practical finding and contrasts to the undesired skin accumulation occasionally reported for polyanionic dyes.[39] In other words, zwitterionic **650z** is an excellent choice as an untargeted probe with 710 nm emission for many future PAI applications. The normalized organ-to-muscle MPI data in Figure 3 indicate substantial accumulation of each targeted s775z probe in the tumor tissue with each probe producing a tumor-to-muscle MPI value >10, which is well above the benchmark of 3 that is recommended for an effective fluorescence-guided surgery.[40] The analysis also indicates moderate accumulation of the NIR fluorescent targeted probes in the liver, spleen, kidneys, and skin which is often observed with cRGDfK-based probes.[41] This is likely due to the constitutive expression of integrins in the endothelium of the liver and spleen, the epidermis of the skin, and the tubular epithelial cells of the kidney.[42−44] An expansion of the biodistribution data, focusing on the normalized MPI for untargeted **650z** and each of the three targeted probes in the excised tumor or kidney tissue is shown in Figure S22. The increased accumulation of the three targeted probes in the tumor tissue reflects an overexpression of integrin receptors on the surface of the cancer cells and tumor neovasculature.[23] In total, the biodistribution data for the three targeted NIR fluorescent probes reveal two small but statistically significant differences suggesting a minor linker effect: (a) **s775z-aRGD** exhibited higher tumor selectivity than the other two targeted probes and (b) there was higher accumulation of **s775z-tRGD** in the kidneys compared to the other two targeted probes. The off-target kidney accumulation of **s775z-tRGD** would obviously be undesired if the goal was to image tumors in a proximal location. Moreover, it potentially could be a source of nephrotoxicity, although this would be unlikely in a single low dose procedure such as that used here.

As fluorescent dyes for bioconjugation, the data suggest that **s775z**, **s775z-maleimide**, or **s775z-alkyne** can be used interchangeably to synthesize homologous targeted NIR fluorescent probes with the same high fluorescence brightness and very similar targeting effectiveness. The three homologous cRGDfK probes studied here did not exhibit any obvious stability difference over the short, 3 h time frame of the mouse imaging experiments. However, it is worth noting that the thiosuccinimide linker formed by addition of a thiol to a maleimide is known to be slowly cleaved by oxidation or

https://doi.org/10.1021/acsomega.1c04991
ACS Omega 2021, 6, 30130−30139

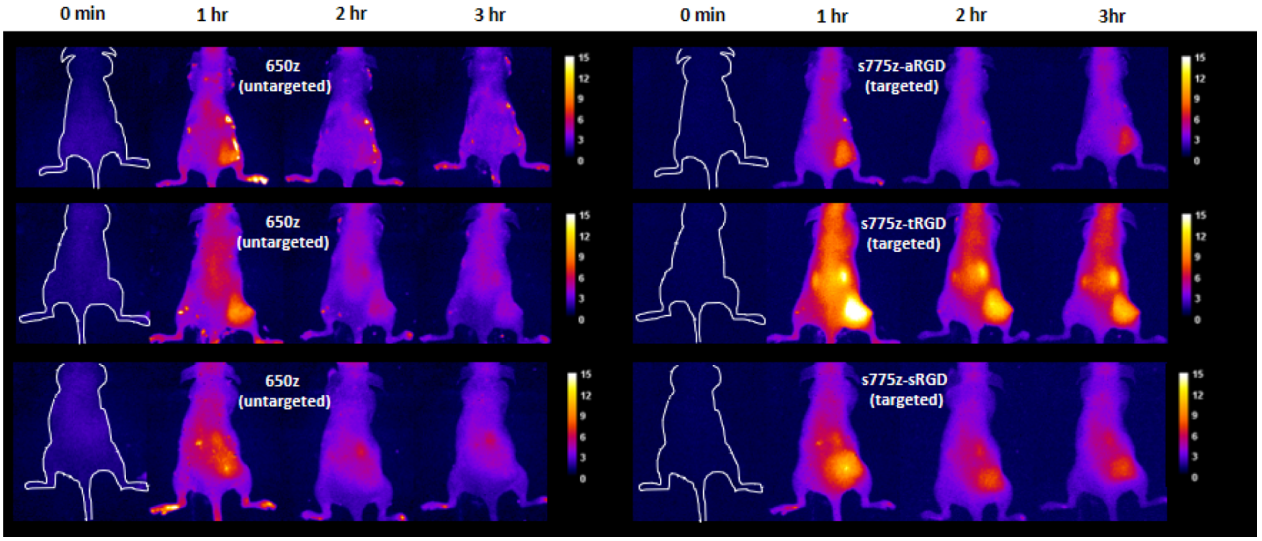

Figure 2. Representative fluorescent images of three tumor bearing mice assessed by PAI (each row shows multiple images of the same mouse and is representative of $N = 5$). Each mouse was injected intravenously with a binary 1:1 mixture of untargeted probe **650z** and one of the targeted **s775z** probes (**s775z-aRGD**, **s775z-tRGD** or **s775z-sRGD**) (total probe dose is 20 nmol/mouse). Images were obtained periodically using two different filter settings (left panel, untargeted **650z**, ex: 640/20 nm, em: 710/20 nm, exposure time: 3 s, percent power: 50%, F-stop: 2, FOV: 20, binning—low), and (right panel, targeted **s775z** probe, ex: 745/20 nm, em: 850/20 nm, exposure time: 3 s, percent power: 50%, F-stop: 2, FOV: 20, binning—low)]. Intensity scale is in arbitrary fluorescent units.

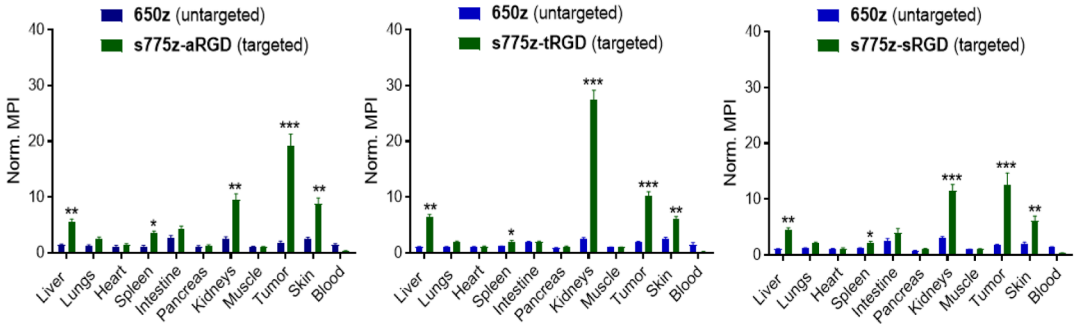

Figure 3. Biodistribution of untargeted **650z** and each of the three targeted NIR fluorescent s775z probes in tumor bearing mice (for each probe, $N = 5$). For each excised organ, the MPI for untargeted and targeted probe was measured and normalized to the thigh muscle MPI from the same animal. Error bars indicate ±SEM. p values indicate probability that untargeted and targeted MPI values are equal, $^{*}p < 0.05$, $^{**}p < 0.01$, $^{***}p < 0.001$.

elimination processes.[45−47] Thus, potential linker instability should be kept in mind when dye-labeled bioconjugates are prepared using **s775z-maleimide**.

A comparison of all the *ex vivo* images of the excised tumors as maps of pixel intensity at 710 and 850 nm emission wavelengths is shown in Figure 4a. The images clearly indicate higher tumor accumulation of the three separate s775z probes compared to the co-injected untargeted **650z** probe. One of the attractive analysis features of PAI is the capability to extract a quantitative measure of the biomarker targeting effectiveness.[34,36] In this current study, we used the straightforward, single time point analysis method of Tichauer and co-workers to determine the average binding potential (BP) for each targeted probe in the tumor and muscle tissue harvested from each mouse.[48] BP is a dimensionless value whose magnitude is determined primarily by two parameters, (a) the abundance of the integrin receptors within the tumor or muscle tissue, and (b) the probe's affinity for the integrin receptors. As shown by the plots on the left of in Figure 4b, the three targeted probes exhibit very similar average BP values. That is, the average BP was ≥1 for the tumor tissue, reflecting a combination of high overexpression of integrin receptors and high probe affinity for the receptors.[25] In contrast, the average BP was close to zero for muscle tissue, reflecting a negligible integrin expression level. On the right side of Figure 4b are image maps illustrating the BP for each pixel in the images. Inspection of the pixelated maps reveals (a) tumor-to-tumor variation in average BP and (b) heterogeneous spatial distribution of BP within each tumor. We observed similar heterogenous maps of BP in a previous PAI study of the same tumor model using a different set of targeted and untargeted fluorescent probes,[25] and the most likely explanation is a heterogeneous distribution of integrin receptors throughout the tumor tissue. Integrins are transmembrane signaling receptors that mediate the adhesive properties of epithelial cells and thus modulate cell growth and differentiation. Clinical cancer researchers continue to search for correlations between altered integrin expression and disease progression and a common literature approach is to image histology sections using immunofluorescence microscopy.[49−52] PAI is emerging as a sensitive technique for this type of biomarker detection and distribution mapping,[53−56] and future research studies will determine the feasibility of PAI protocols

https://doi.org/10.1021/acsomega.1c04991
ACS Omega 2021, 6, 30130−30139

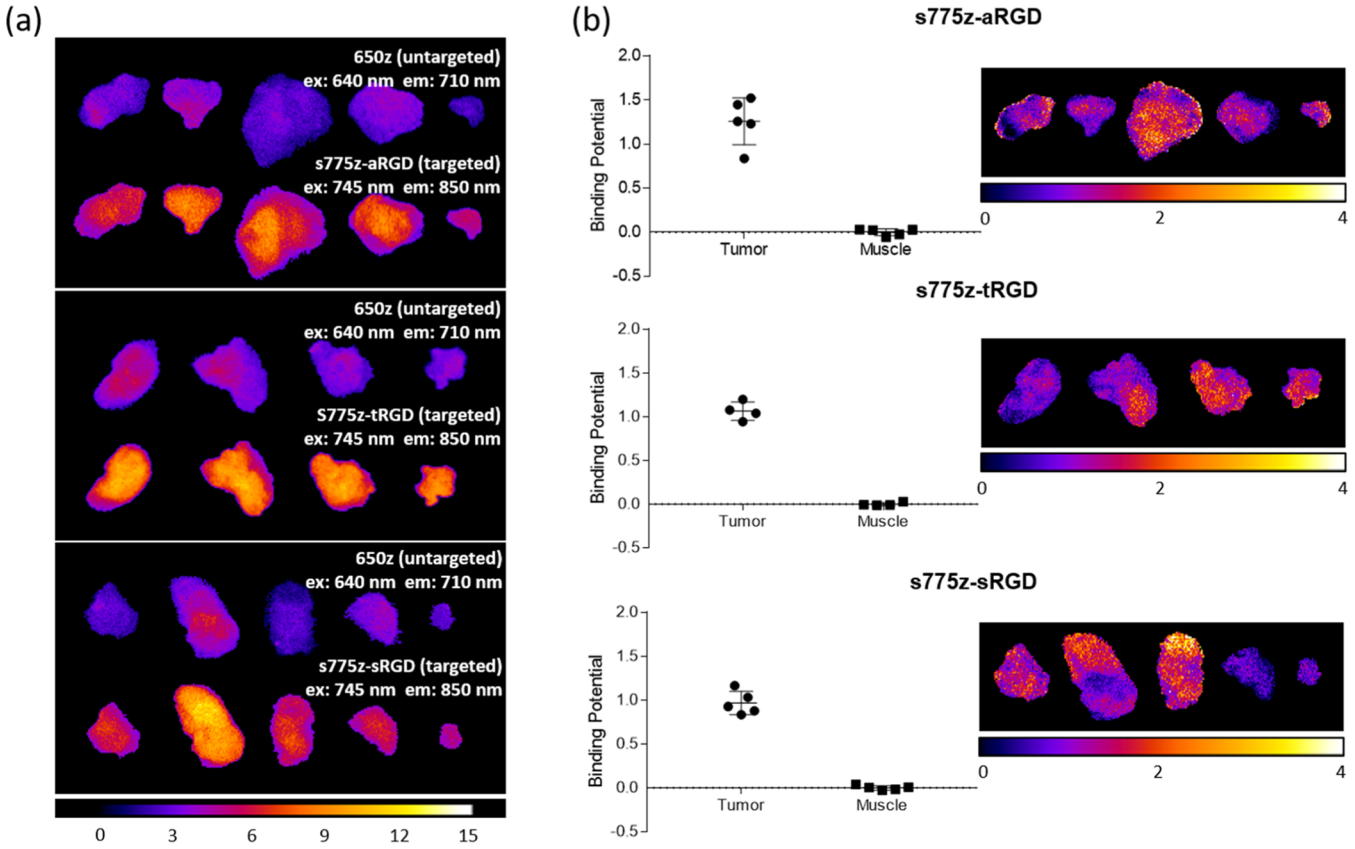

Figure 4. (a) Fluorescent images of harvested tumors from mice that were sacrificed at 3 h after co-injection of untargeted **650z** probe and one of the three targeted s775z probes. Fluorescence filter settings for the untargeted dye (ex: 640/20 nm, em: 710/20 nm, exposure time: 3 s, percent power: 50%, F-stop: 2, FOV: 20, binning—low) and targeted probe (ex: 745/20 nm, em: 850/20 nm, exposure time: 3 s, percent power: 50%, F-stop: 2, FOV: 20, binning—low) and the fluorescence intensity scale is in arbitrary units. (b) (left) Plots of tumor and muscle BP for each s775z probe in the excised tumor and muscle tissue harvested from each mouse (N = 5). (right) Pixel intensity maps showing the heterogenous distribution of BP for each s775z probe in the excised tumors.

that stain tissue sections with the new fluorescent probes developed in this study.[57]

CONCLUSIONS

This is the third research publication describing the favorable properties of sterically shielded NIR fluorescent cyanine dye **s775z** (Scheme 1).[21,22] The chemical structure of **s775z** has two short shielding arms that prevent dye self-aggregation, but they do not block association of bioconjugates with their targets. In addition, **s775z** possesses a geometric distribution of opposing charge that lowers association with off-target proteins and cell membranes, which in turn minimizes nonspecific cell permeation and cytotoxicity. Recently, the NHS ester of **s775z** has become commercially available as a reagent for amide-based bioconjugation,[58] and it has been used to label lysine residues on the surface of antibodies to give NIR fluorescent antibodies with an unsurpassed combination of high photostability and fluorescence brightness.[22] This present contribution reports two new reactive homologues, namely, **s775z-maleimide** which reacts with a thiol group, and **s775z-alkyne** which reacts with an azide group. Three cancer-targeting NIR fluorescent probes (**s775z-aRGD**, **s775z-tRGD**, and **s775z-sRGD**) were prepared, each with an appended cRGDfK peptide to provide a selective affinity for integrin receptors that are overexpressed in many tumors. A set of systematic cancer cell microscopy and mouse tumor imaging experiments compared the NIR fluorescence imaging performance of the three targeted probes with 850 nm emission. The mouse imaging study employed a PAI method that co-injected the zwitterionic cyanine dye **650z** as an untargeted probe with 710 nm emission. The three different targeted probes exhibited some statistically significant differences in mouse biodistribution (Figure 3), but in all cases, the cancer targeting was very effective. It is very likely that **s775z**, **s775z-maleimide**, or **s775z-alkyne** can be interchanged in homologous bioconjugation reactions without any significant change in fluorescent probe targeting effectiveness. The high tumor-to-background ratios facilitated a mock surgical procedure that excised the subcutaneous tumors. Peptide-based fluorescent probes such as the ones in this study are attractive for a fluorescence-guided surgery because they have higher fluorescence density at the target site and much shorter blood clearance times than analogous antibody probes.[59] Analysis of the PAI data permitted determination of BP as a quantitative measure of integrin targeting effectiveness for each targeted probe in the tumor and muscle tissue. The pixelated maps of BP (Figure 4) reflect tumor-to-tumor variation in average BP, and a heterogeneous spatial distribution of BP within each tumor. In addition to *in vivo* PAI, it may be possible to incorporate the fluorescent probes reported in this study into new PAI methods that quantify integrin expression in tumor pathology.

https://doi.org/10.1021/acsomega.1c04991
ACS Omega 2021, 6, 30130−30139

EXPERIMENTAL SECTION

Chemical Synthesis and Compound Characterization. The synthesis and spectral characterization of all bioconjugates and reaction intermediates is provided as Supporting Information.

Albumin Association Measurements. Albumin association constants were measured using a standard titration procedure that added aliquots of **s775z**, **s775z-aRGD**, **s775z-tRGD**, or **s775z-sRGD** to a solution of BSA (Sigma-Aldrich A964) and monitored quenching of the single tryptophan in the BSA. Aliquots (4 μL) of 1 mM stock of each s775z probe was separately added to 2 mL of 2 μM BSA in ultrapure water varying the concentration from 0 to 20 μM at 37 °C. Five minutes after each addition, BSA tryptophan fluorescence intensity was acquired (excitation: 280 nm; slit width: 2 nm). The relative fluorescent intensity F was calculated using the equation $[(F_0 - F)/F]$ where F_0 = initial fluorescence intensity and F = fluorescent intensity after each free dye/bioconjugate addition. The measurements were plotted as a function of the dye concentrations to obtain association constants K_a using GraphPad Prism where $m = K_a \pm$ SD.

Cell Culture Conditions. A549 human lung adenocarcinoma cells (ATCC CCL-185) were cultured in F-12K media (ATCC 30-2004) supplemented with 10% fetal bovine serum (Atlanta Biologicals) and 1% penicillin/streptomycin (Sigma-Aldrich) and maintained at 37 °C and 5% CO_2 in a humidified incubator. Cell authentication experiments using fluorescent antibodies confirmed that the cells expressed the $\alpha_v\beta_5$ integrin receptor.[31]

Cell Toxicity Studies. A549 cells were seeded into 96-microwell plates (Greiner Bio-One CELLSTAR) at a seeding density of 1.98×10^5 cells per well and grown to 70% confluency in F-12K media (48 h). The media were then removed and replaced with a solution of the s775z probe (**s775z-aRGD**, **s775z-tRGD**, or **s775z-sRGD**) in F-12K media at various micromolar concentrations (0−30 μM) for 24 h at 37 °C and 5% CO_2 in a humidified incubator (N = 3). After, 24 h, the dye-bioconjugate was removed and replaced with growth medium containing [3-(4,5-dimethylthiazol-2-yl)-2,5-diphenyltetrazolium bromide]/MTT, 1.1 mM). After a 4 h incubation at 37 °C and 5% CO_2, a detergent solution (sodium dodecyl sulfate in dimethyl sulfoxide) was added to the MTT-growth medium. The samples were incubated overnight, and the absorbance of each well was measured at 590 nm using a plate reader. The readings were normalized to untreated cells, and all measurements were made in triplicate.

Cell Microscopy. A549 cells were seeded and grown to 70% confluency on an 8-well chambered cover glass (Lab-Tek, Nunc, USA). The medium was replaced with 10 μM **s775z-aRGD**, **s775z-tRGD**, or **s775z-sRGD** separately in media for 1 h at 37 °C and 5% CO_2 in a humidified incubator. For blocking studies, 200 μM of cRGDfK was added to the cells 20 min before the probe treatment. At the end of dye incubation, cells were washed twice with 1XPBS and fixed with 4% cold paraformaldehyde for 20 min at room temperature. After a single wash with 1XPBS, cells were co-stained with 3 μM Hoechst 33342 for 10 min. After a single wash of 1XPBS, cells were imaged using a Zeiss Axiovert 100 TV epifluorescence microscope under a UV filter (ex: 387/11, em: 447/60) and ICG filter (ex: 769/41, em: 832/37). For each micrograph, a background subtraction with a rolling ball radius of 50 pixels was applied using ImageJ2 software. After calculating average MPI of green false color which provided averages and scanning electron microscopy, GraphPad Prism was used to plot the data. For each condition, a total of nine micrographs were analyzed. Experiments were conducted in triplicates.

***In Vivo* and *ex Vivo* Paired-Agent Imaging.** All *in vivo* experiments followed a protocol that was approved by the Notre Dame Institutional Animal Care and Use Committee. Female SH1 nude mice (N = 15) were treated with a mixture of A549 cells (1×10^6) and matrigel (1:1). Five weeks later, the mice were randomly separated into three cohorts (N = 5). Five minutes before the injection procedure, each mouse was placed under 2−3% isoflurane anesthesia with an oxygen flow rate of 2 L per min and imaged using two filter channels, the 710 nm channel for the untargeted probe **650z** (ex: 640/20 nm, em: 710/20 nm, exposure: 3 s, percent power: 50%, F-stop: 2, FOV: 20, binning: low) and the 850 nm channel for the three targeted 775 probes (ex: 745/20 nm, em: 850/20 nm, exposure: 3 s, percent power: 50%, F-stop: 2, FOV: 20, binning: low) on an *in vivo* image station (Ami HT Spectral Imaging). It is worth noting that the excitation and emission maxima for all three targeted 775 probes are essentially the same (Table 1) and do not exactly match the 850 channel settings of the in vivo imaging station. While the detection sensitivity is nonoptimal, the amount of brightness attenuation is the same for all three targeted probes; thus, the fluorescent image intensities can be directly compared without any need to correct for variation in targeted probe brightness. Simultaneous imaging of the two co-injected probes at the two distinct wavelengths (untargeted at 710 nm and targeted at 850 nm) enables the fluorescent targeted probe image to be digitally corrected by subtracting the fluorescent untargeted probe image, which eliminates imaging artifacts due to probe retention by untargeted dynamic effects.

After mouse retro-orbital co-injection with a 100 μL dose containing a binary mixture of one of the targeted probes (**s775z-aRGD**, **s775z-tRGD** or **s775z-sRGD**) and untargeted probe **650z** (total probe dose is 20 nmol/mouse) in saline, each mouse was imaged at 0, 1, 2 and 3 h time points. The tumor-to-background ratio for each living mouse image was calculated at each time point by analyzing the MPI of an arbitrarily selected region of interest (ROI) drawn around the tumor or the opposite flank in equal size. After three hours, the mice were anesthetized and sacrificed by cervical dislocation followed by immediate collection of blood from the heart. Next, a mock surgery was performed to harvest all the major organs including the liver, lungs, heart, spleen, intestine, pancreas, kidneys, skin, and muscles. Before the surgery, the mice were imaged, first with the tumor exposed by removing the surrounding skin, and then after excising the tumor from the body. The excised tumors and organs were imaged on a transparent plastic tray under the two filter settings described above. For image processing, the mouse body and the excised tumor images were false-colored "fire" using ImageJ2 software. An arbitrary maximum fluorescence value was chosen for the analysis. For the biodistribution and *ex vivo* tumor analyses, the images of excised tumor and organs were imported to ImageJ2, and a manually drawn ROI was created around each fluorescent image. The MPI of each tumor or organ was divided by the MPI of the thigh muscle from the same mouse to give a normalized MPI.

The BP of each targeted probe in a sample of tumor or muscle tissue was determined by a single time point PAI

https://doi.org/10.1021/acsomega.1c04991
ACS Omega 2021, 6, 30130−30139

method using the following equation,[48] where ROI is the measured MPI value within a ROI for: (a) one of the targeted s775z probes and (b) the untargeted probe, **650z**.

$$\mathrm{BP} = \frac{\mathrm{ROI}_{\mathrm{targetedprobe}} - \mathrm{ROI}_{\mathrm{untargetedprobe}}}{\mathrm{ROI}_{\mathrm{untargetedprobe}}}$$

To determine the average BP for an excised sample of tumor or muscle tissue, a ROI was manually drawn around the entire excised sample. To determine a pixelated map of BP distribution within an excised sample, each pixel within the sample was designated a ROI.

■ ASSOCIATED CONTENT

Supporting Information

The Supporting Information is available free of charge at https://pubs.acs.org/doi/10.1021/acsomega.1c04991.

Synthesis and compound characterization; photophysical data; dye/BSA association studies; MTT cell viability assays of **s775z-aRGD**, **s775z-sRGD**, and **s775z-tRGD**; fluorescent and brightfield images of syringes; (a) tumor mean pixel intensity (MPI), and (b) tumor-to-background ratio; mock surgery process; and expansion of the biodistribution data (PDF)

■ AUTHOR INFORMATION

Corresponding Author

Bradley D. Smith − *Department of Chemistry and Biochemistry, University of Notre Dame, Notre Dame, Indiana 46556-5670, United States;* orcid.org/0000-0003-4120-3210; Email: smith.115@nd.edu

Authors

Rananjaya S. Gamage − *Department of Chemistry and Biochemistry, University of Notre Dame, Notre Dame, Indiana 46556-5670, United States*

Dong-Hao Li − *Department of Chemistry and Biochemistry, University of Notre Dame, Notre Dame, Indiana 46556-5670, United States;* orcid.org/0000-0003-2556-1624

Cynthia L. Schreiber − *Department of Chemistry and Biochemistry, University of Notre Dame, Notre Dame, Indiana 46556-5670, United States*

Complete contact information is available at: https://pubs.acs.org/10.1021/acsomega.1c04991

Notes

The authors declare the following competing financial interest(s): The authors declare the following potential competing financial interest: B.D.S and D.-H.L. have filed a provisional patent application involving shielded cyanine dyes, whose value might be affected by this publication.

■ ACKNOWLEDGMENTS

The authors are grateful for funding support from the US NIH (R35GM136212 and T32GM075762) and a Berry Family Foundation fellowship from the University of Notre Dame. The authors thank Janeala Morsby for expert assistance during the mouse imaging studies.

■ REFERENCES

(1) Wang, W.; Hu, Z. Targeting Peptide-Based Probes for Molecular Imaging and Diagnosis. *Adv. Mater.* **2019**, *31*, 1804827.

(2) Mendive-Tapia, L.; Wang, J.; Vendrell, M. Fluorescent Cyclic Peptides for Cell Imaging. *Pept. Sci.* **2020**, *113*, No. e24181.

(3) Zhang, P.; Cui, Y.; Anderson, C. F.; Zhang, C.; Li, Y.; Wang, R.; Cui, H. Peptide-Based Nanoprobes for Molecular Imaging and Disease Diagnostics. *Chem. Soc. Rev.* **2018**, *47*, 3490−3529.

(4) Sun, W.; Guo, S.; Hu, C.; Fan, J.; Peng, X. Recent Development of Chemosensors Based on Cyanine Platforms. *Chem. Rev.* **2016**, *116*, 7768−7817.

(5) Li, Y.; Zhou, Y.; Yue, X.; Dai, Z. Cyanine Conjugate-Based Biomedical Imaging Probes. *Adv. Healthcare Mater.* **2020**, *9*, 2001327.

(6) Gao, M.; Yu, F.; Lv, C.; Choo, J.; Chen, L. Fluorescent Chemical Probes for Accurate Tumor Diagnosis and Targeting Therapy. *Chem. Soc. Rev.* **2017**, *46*, 2237−2271.

(7) Simpson, J. D.; Monteiro, P. F.; Ediriweera, G. R.; Prior, A. R.; Sonderegger, S. E.; Bell, C. A.; Fletcher, N. L.; Alexander, C.; Thurecht, K. J. Fluorophore Selection and Incorporation Contribute to Permeation and Distribution Behaviors of Hyperbranched Polymers in Multi-Cellular Tumor Spheroids and Xenograft Tumor Models. *ACS Appl. Bio Mater.* **2021**, *4*, 2675−2685.

(8) Cavaco, M.; Pérez-Peinado, C.; Valle, J.; Silva, R. D. M.; Correia, J. D. G.; Andreu, D.; Castanho, M. A. R. B.; Neves, V. To What Extent Do Fluorophores Bias the Biological Activity of Peptides? A Practical Approach Using Membrane-Active Peptides as Models. *Front. Bioeng. Biotechnol.* **2020**, *8*, 552035.

(9) Sato, K.; Gorka, A. P.; Nagaya, T.; Michie, M. S.; Nani, R. R.; Nakamura, Y.; Coble, V. L.; Vasalatiy, O. V.; Swenson, R. E.; Choyke, P. L.; et al. Role of Fluorophore Charge on the in Vivo Optical Imaging Properties of Near-Infrared Cyanine Dye/Monoclonal Antibody Conjugates. *Bioconjugate Chem.* **2016**, *27*, 404−413.

(10) Usama, S. M.; Thapaliya, E. R.; Luciano, M. P.; Schnermann, M. J. Not so Innocent: Impact of Fluorophore Chemistry on the in Vivo Properties of Bioconjugates. *Curr. Opin. Chem. Biol.* **2021**, *63*, 38−45.

(11) Buckle, T.; Van Willigen, D. M.; Spa, S. J.; Hensbergen, A. W.; Van Der Wal, S.; De Korne, C. M.; Welling, M. M.; Van Der Poel, H. G.; Hardwick, J. C. H.; Van Leeuwen, F. W. B. Tracers for Fluorescence-Guided Surgery: How Elongation of the Polymethine Chain in Cyanine Dyes Alters the Pharmacokinetics of a Dual-Modality c[RGDyK] Tracer. *J. Nucl. Med.* **2018**, *59*, 986−992.

(12) Ma, X.; Laramie, M.; Henary, M. Synthesis, Optical Properties and Cytotoxicity of Meso-Heteroatom Substituted IR-786 Analogs. *Bioorg. Med. Chem. Lett.* **2018**, *28*, 509−514.

(13) Usama, S. M.; Burgess, K. Hows and Whys of Tumor-Seeking Dyes. *Acc. Chem. Res.* **2021**, *54*, 2121−2131.

(14) Luo, S.; Zhang, E.; Su, Y.; Cheng, T.; Shi, C. A Review of NIR Dyes in Cancer Targeting and Imaging. *Biomaterials* **2011**, *32*, 7127−7138.

(15) Choi, P. J.; Park, T. I. H.; Cooper, E.; Dragunow, M.; Denny, W. A.; Jose, J. Heptamethine Cyanine Dye Mediated Drug Delivery: Hype or Hope. *Bioconjugate Chem.* **2020**, *31*, 1724−1739.

(16) Sato, K.; Nagaya, T.; Nakamura, Y.; Harada, T.; Nani, R. R.; Shaum, J. B.; Gorka, A. P.; Kim, I.; Paik, C. H.; Choyke, P. L.; et al. Impact of C4′-O-Alkyl Linker on in Vivo Pharmacokinetics of Near-Infrared Cyanine/Monoclonal Antibody Conjugates. *Mol. Pharm.* **2015**, *12*, 3303−3311.

(17) Luciano, M. P.; Crooke, S. N.; Nourian, S.; Dingle, I.; Nani, R. R.; Kline, G.; Patel, N. L.; Robinson, C. M.; Difilippantonio, S.; Kalen, J. D.; et al. A Nonaggregating Heptamethine Cyanine for Building Brighter Labeled Biomolecules. *ACS Chem. Biol.* **2019**, *14*, 934−940.

(18) Yang, C.; Wang, H.; Yokomizo, S.; Hickey, M.; Chang, H.; Kang, H.; Fukuda, T.; Song, M. Y.; Lee, S. Y.; Park, J. W.; et al. ZW800-PEG: A Renal Clearable Zwitterionic Near-Infrared Fluorophore for Potential Clinical Translation. *Angew. Chem., Int. Ed.* **2021**, *60*, 13847−13852.

(19) Choi, H. S.; Nasr, K.; Alyabyev, S.; Feith, D.; Lee, J. H.; Kim, S. H.; Ashitate, Y.; Hyun, H.; Patonay, G.; Strekowski, L.; et al. Synthesis and in Vivo Fate of Zwitterionic Near-Infrared Fluorophores. *Angew. Chem., Int. Ed.* **2011**, *50*, 6258−6263.

(20) Choi, H. S.; Gibbs, S. L.; Lee, J. H.; Kim, S. H.; Ashitate, Y.; Liu, F.; Hyun, H.; Park, G.; Xie, Y.; Bae, S.; et al. Targeted Zwitterionic Near-Infrared Fluorophores for Improved Optical Imaging. *Nat. Biotechnol.* **2013**, *31*, 148−153.
(21) Li, D. H.; Schreiber, C. L.; Smith, B. D. Sterically Shielded Heptamethine Cyanine Dyes for Bioconjugation and High Performance Near-Infrared Fluorescence Imaging. *Angew. Chem., Int. Ed.* **2020**, *59*, 12154−12161.
(22) Schreiber, C. L.; Li, D.-H.; Smith, B. D. High-Performance Near-Infrared Fluorescent Secondary Antibodies for Immunofluorescence. *Anal. Chem.* **2021**, *93*, 3643−3651.
(23) Hatley, R. J. D.; Macdonald, S. J. F.; Slack, R. J.; Le, J.; Ludbrook, S. B.; Lukey, P. T. An αv-RGD Integrin Inhibitor Toolbox: Drug Discovery Insight, Challenges and Opportunities. *Angew. Chem., Int. Ed.* **2018**, *57*, 3298−3321.
(24) Cañeque, T.; Müller, S.; Rodriguez, R. Visualizing Biologically Active Small Molecules in Cells Using Click Chemistry. *Nat. Rev. Chem.* **2018**, *2*, 202−215.
(25) Schreiber, C. L.; Zhai, C.; Dempsey, J. M.; Mcgarraugh, H. H.; Matthews, B. P.; Christmann, C. R.; Smith, B. D. Paired Agent Fluorescence Imaging of Cancer in a Living Mouse Using Preassembled Squaraine Molecular Probes with Emission Wavelengths of 690 and 830 nm. *Bioconjugate Chem.* **2020**, *31*, 214−223.
(26) Sun, Y.; Ma, X.; Cheng, K.; Wu, B.; Duan, J.; Chen, H.; Bu, L.; Zhang, R.; Hu, X.; Deng, Z.; et al. Strained Cyclooctyne as a Molecular Platform for Construction of Multimodal Imaging Probes. *Angew. Chem., Int. Ed.* **2015**, *127*, 6079−6082.
(27) Li, H.; Zhou, H.; Krieger, S.; Parry, J. J.; Whittenberg, J. J.; Desai, A. V.; Rogers, B. E.; Kenis, P. J. A.; Reichert, D. E. Triazine-Based Tool Box for Developing Peptidic PET Imaging Probes: Syntheses, Microfluidic Radiolabeling, and Structure-Activity Evaluation. *Bioconjugate Chem.* **2014**, *25*, 761−772.
(28) Jain, N.; Smith, S. W.; Ghone, S.; Tomczuk, B. Current ADC Linker Chemistry. *Pharm. Res.* **2015**, *32*, 3526−3540.
(29) Hyun, H.; Henary, M.; Gao, T.; Narayana, L.; Owens, E. A.; Lee, J. H.; Park, G.; Wada, H.; Ashitate, Y.; Frangioni, J. V.; et al. 700-Nm Zwitterionic Near-Infrared Fluorophores for Dual-Channel Image-Guided Surgery. *Mol. Imag. Biol.* **2016**, *18*, 52−61.
(30) Berezin, M. Y.; Guo, K.; Akers, W.; Livingston, J.; Solomon, M.; Lee, H.; Liang, K.; Agee, A.; Achilefu, S. Rational Approach To Select Small Peptide Molecular Probes Labeled With Fluorescent Cyanine Dyes For In Vivo Optical Imaging. *Biochemistry* **2011**, *50*, 2691−2700.
(31) Shaw, S. K.; Liu, W.; Gómez Durán, C. F. A.; Schreiber, C. L.; Betancourt Mendiola, M. d. L.; Zhai, C.; Roland, F. M.; Padanilam, S. J.; Smith, B. D. Non-Covalently Pre-Assembled High-Performance Near-Infrared Fluorescent Molecular Probes for Cancer Imaging. *Chem.—Eur. J.* **2018**, *24*, 13821−13829.
(32) Mu, H.; Miki, K.; Harada, H.; Tanaka, K.; Nogita, K.; Ohe, K. pH-Activatable Cyanine Dyes for Selective Tumor Imaging Using Near-Infrared Fluorescence and Photoacoustic Modalities. *ACS Sens.* **2020**, *6*, 123−129.
(33) Liu, S.; Song, W.; Gao, X.; Su, Y.; Gao, E.; Gao, Q. Discovery of Nonpeptide, Reversible HER1/HER2 Dual-Targeting Small-Molecule Inhibitors as Near-Infrared Fluorescent Probes for Efficient Tumor Detection, Diagnostic Imaging, and Drug Screening. *Anal. Chem.* **2019**, *91*, 1507−1515.
(34) Sadeghipour, N.; Davis, S. C.; Tichauer, K. M. Generalized paired-agent kinetic model forin vivoquantification of cancer cell-surface receptors under receptor saturation conditions. *Phys. Med. Biol.* **2017**, *62*, 394−414.
(35) Tichauer, K. M.; Wang, Y.; Pogue, B. W.; Liu, J. T. C. Quantitativein vivocell-surface receptor imaging in oncology: kinetic modeling and paired-agent principles from nuclear medicine and optical imaging. *Phys. Med. Biol.* **2015**, *60*, R239−R269.
(36) Tichauer, K. M.; Samkoe, K. S.; Sexton, K. J.; Hextrum, S. K.; Yang, H. H.; Klubben, W. S.; Gunn, J. R.; Hasan, T.; Pogue, B. W. In Vivo Quantification of Tumor Receptor Binding Potential with Dual-Reporter Molecular Imaging. *Mol. Imag. Biol.* **2012**, *14*, 584−592.
(37) Pogue, B. W.; Samkoe, K. S.; Hextrum, S.; O'Hara, J. A.; Jermyn, M.; Srinivasan, S.; Hasan, T. Imaging Targeted-Agent Binding in Vivo with Two Probes. *J. Biomed. Opt.* **2010**, *15*, 030513.
(38) Kanick, S. C.; Tichauer, K. M.; Gunn, J.; Samkoe, K. S.; Pogue, B. W. Pixel-Based Absorption Correction for Dual-Tracer Fluorescence Imaging of Receptor Binding Potential. *Biomed. Opt Express* **2014**, *5*, 3280.
(39) Zhu, S.; Hu, Z.; Tian, R.; Yung, B. C.; Yang, Q.; Zhao, S.; Kiesewetter, D. O.; Niu, G.; Sun, H.; Antaris, A. L.; et al. Repurposing Cyanine NIR-I Dyes Accelerates Clinical Translation of Near-Infrared-II (NIR-II) Bioimaging. *Adv. Mater.* **2018**, *30*, 1802546.
(40) Samkoe, K. S.; Bates, B. D.; Elliott, J. T.; Larochelle, E.; Gunn, J. R.; Marra, K.; Feldwisch, J.; Ramkumar, D. B.; Bauer, D. F.; Paulsen, K. D.; et al. Application of Fluorescence-Guided Surgery to Subsurface Cancers Requiring Wide Local Excision: Literature Review and Novel Developments Toward Indirect Visualization. *Cancer Control* **2018**, *25*, 1073274817752332.
(41) Jin, Z.-H.; Furukawa, T.; Degardin, M.; Sugyo, A.; Tsuji, A. B.; Yamasaki, T.; Kawamura, K.; Fujibayashi, Y.; Zhang, M.-R.; Boturyn, D.; et al. αVβ3 Integrin-Targeted Radionuclide Therapy with 64Cu-cyclam-RAFT-c(-RGDfK-)4. *Mol. Cancer Ther.* **2016**, *15*, 2076−2085.
(42) Hegde, S.; Raghavan, S. A Skin-Depth Analysis of Integrins: Role of the Integrin Network in Health and Disease. *Cell Commun. Adhes.* **2013**, *20*, 155−169.
(43) Natarajan, V.; Harris, E. N.; Kidambi, S. SECs (Sinusoidal Endothelial Cells), Liver Microenvironment, and Fibrosis. *BioMed Res. Int.* **2017**, *2017*, 1.
(44) White, L. R.; Blanchette, J. B.; Ren, L.; Awn, A.; Trpkov, K.; Muruve, D. A. The characterization of α5-integrin expression on tubular epithelium during renal injury. *Am. J. Physiol. Ren. Physiol.* **2007**, *292*, F567−F576.
(45) Fishkin, N.; Maloney, E. K.; Chari, R. V. J.; Singh, R. A Novel Pathway for Maytansinoid Release from Thioether Linked Antibody-Drug Conjugates (ADCs) under Oxidative Conditions. *Chem. Commun.* **2011**, *47*, 10752−10754.
(46) Baldwin, A. D.; Kiick, K. L. Tunable Degradation of Maleimide-Thiol Adducts in Reducing Environments. *Bioconjugate Chem.* **2011**, *22*, 1946−1953.
(47) Alley, S. C.; Benjamin, D. R.; Jeffrey, S. C.; Okeley, N. M.; Meyer, D. L.; Sanderson, R. J.; Senter, P. D. Contribution of Linker Stability to the Activities of Anticancer Immunoconjugates. *Bioconjugate Chem.* **2008**, *19*, 759−765.
(48) Tichauer, K. M.; Samkoe, K. S.; Sexton, K. J.; Gunn, J. R.; Hasan, T.; Pogue, B. W. Improved Tumor Contrast Achieved by Single Time Point Dual-Reporter Fluorescence Imaging. *J. Biomed. Opt.* **2012**, *17*, 066001.
(49) Vay, C.; Hosch, S. B.; Stoecklein, N. H.; Klein, C. A.; Vallböhmer, D.; Link, B.-C.; Yekebas, E. F.; Izbicki, J. R.; Knoefel, W. T.; Scheunemann, P. Integrin Expression in Esophageal Squamous Cell Carcinoma: Loss of the Physiological Integrin Expression Pattern Correlates with Disease Progression. *PLoS One* **2014**, *9*, No. e109026.
(50) Heß, K.; Böger, C.; Behrens, H.-M.; Röcken, C. Correlation between the Expression of Integrins in Prostate Cancer and Clinical Outcome in 1284 Patients. *Ann. Diagn. Pathol.* **2014**, *18*, 343−350.
(51) Zhang, C.; Jugold, M.; Woenne, E. C.; Lammers, T.; Morgenstern, B.; Mueller, M. M.; Zentgraf, H.; Bock, M.; Eisenhut, M.; Semmler, W.; et al. Specific Targeting of Tumor Angiogenesis by RGD-Conjugated Ultrasmall Superparamagnetic Iron Oxide Particles Using a Clinical 1.5-T Magnetic Resonance Scanner. *Cancer Res.* **2007**, *67*, 1555−1562.
(52) Schnell, O.; Krebs, B.; Carlsen, J.; Miederer, I.; Goetz, C.; Goldbrunner, R. H.; Wester, H.-J.; Haubner, R.; Pöpperl, G.; Holtmannspötter, M.; et al. Imaging of integrin αvβ3 expression in patients with malignant glioma by [18F] Galacto-RGD positron emission tomography. *Neuro Oncol.* **2009**, *11*, 861−870.
(53) Xu, X.; Wang, Y.; Xiang, J.; Liu, J. T. C.; Tichauer, K. M. Rinsing Paired-Agent Model (RPAM) to Quantify Cell-Surface Receptor Concentrations in Topical Staining Applications of Thick Tissues. *Phys. Med. Biol.* **2017**, *62*, 5098−5113.

https://doi.org/10.1021/acsomega.1c04991
ACS Omega 2021, 6, 30130−30139

(54) Li, C.; Torres, V. C.; Xu, X.; Basheer, Y.; Sattar, H. A.; Brankov, J. G.; Tichauer, K. M. Protocol Development of Paired-Agent Fluorescent Imaging to Detect Micrometastases in Resected Breast Lymph Nodes. *SPIE Proceedings*, 2019; Vol. *10862*.
(55) Kang, S.; Xu, X.; Navarro, E.; Wang, Y.; Liu, J. T. C.; Tichauer, K. M. Modeling the Binding and Diffusion of Receptor-Targeted Nanoparticles Topically Applied on Fresh Tissue Specimens. *Phys. Med. Biol.* **2019**, *64*, 045013.
(56) Li, C.; Torres, V. C.; He, Y.; Xu, X.; Basheer, Y.; Papavasiliou, G.; Samkoe, K. S.; Brankov, J. G.; Tichauer, K. M. Intraoperative Detection of Micrometastases in Whole Excised Lymph Nodes Using Fluorescent Paired-Agent Imaging Principles: Identification of a Suitable Staining and Rinsing Protocol. *Mol. Imag. Biol.* **2021**, *23*, 537−549.
(57) Zheng, Y.; Ji, S.; Czerwinski, A.; Valenzuela, F.; Pennington, M.; Liu, S. FITC-Conjugated Cyclic RGD Peptides as Fluorescent Probes for Staining Integrin $\alpha_v\beta_3/\alpha_v\beta_5$ in Tumor Tissues. *Bioconjugate Chem.* **2014**, *25*, 1925−1941.
(58) For commercial supplies of **s775z** and its derivatives, see: www.fluoroprobes.com; www.tocris.com (acessed Oct 29, 2021).
(59) Sadeghipour, N.; Rangnekar, A.; Folaron, M. R.; Strawbridge, R. R.; Samkoe, K. S.; Davis, S. C.; Tichauer, K. M. Prediction of Optimal Contrast Times Post-Imaging Agent Administration to Inform Personalized Fluorescence-Guided Surgery. *J. Biomed. Opt.* **2020**, *25*, 116005.

https://doi.org/10.1021/acsomega.1c04991
ACS Omega 2021, 6, 30130−30139